SYNTHESIS AND CHARACTERIZATION OF NANOCRYSTALLINE CELLULOSE AS REINFORCEMENT IN NITRILE BUTADIENE RUBBER COMPOSITES

MOHAMAD NURUL AZMAN MOHAMMAD TAIB, WAGEEH A. YEHYE and NURHIDAYATULLAILI MUHD JULKAPLI

Nanotechnology and Catalysis Research Centre (NANOCAT), Institute of Postgraduate Studies (IPS), University of Malaya, 50603 Kuala Lumpur, Malaysia

✉ *Corresponding author: Nurhidayatullaili Muhd Julkapli, nurhidayatullaili@um.edu.my*

Received June 3, 2019

In this study, nanocrystalline cellulose (NCC) was produced with different concentrations of hydrochloric acid (HCl) and its surface charge, particle size, crystallinity and thermal properties were assessed. The obtained NCC was then used as reinforcement agent in nitrile butadiene rubber (NBR) composites. The NCC was found to have a particle size less than 100 nm, with surface charge ranging from -0.697 mV to -14.8 mV. The crystallinity index decreased to 64.78% for the NCC obtained with 6M HCl. The NCC synthesized with 1M HCl showed the highest thermal stability, as demonstrated by TGA and DSC results. TEM analysis revealed that the NCC obtained with 5M HCl had the smallest particle size. The addition of different amounts of NCC into nitrile butadiene rubber (NBR) composites led to an enhancement of mechanical properties in terms of tensile strength, modulus and elongation at break up to the loading of 5 phr, but no substantial improvement in tear strength was noticed.

Keywords: nanocrystalline cellulose, acid hydrolysis, characterization, nanoparticle, mechanical properties

INTRODUCTION

Cellulose is a natural polysaccharide that is abundant in nature. Nanocrystalline cellulose (NCC) has many promising characteristics, such as high mechanical tensile strength (0.3-22 GPa), high elastic modulus capacity (58-180 GPa), low density, biodegradability and non-toxicity, and due to this, NCC has become a topic of great research interest in recent years. The final properties of NCC are strongly dependent on its surface area, particle size, molecular weight and degree of crystallinity.[1-4] Acid hydrolysis is one of the possible routes for NCC production, by reducing the cellulose chains. The use of hydrochloric acid (HCl) in acid hydrolysis for NCC production has been reported to result in a significant increase in the active surface area and a smaller particle size of NCC, compared to that produced with other acid catalysts, including sulfuric acid, bromide acid and phosphoric acid.[5-7] This is also supported by several studies that performed the hydrolysis of cellulose from different sources, such as cotton and kenaf fibers, using sulfuric and hydrochloric acid.[8-10] The synthesis of NCC with HCl as a catalyst releases the hydronium (H^+) ion for the hydrolytic cleavage of glycosidic bonds in the cellulosic molecular chains within the amorphous region.

In the acid hydrolysis process, different concentrations of the acid, temperatures and reaction time would lead to NCC with different crystallinity, particle size, molecular weight, yield, surface functionalization and geometry.[11] A study by Bondeson *et al.*[12] reported that using H_2SO_4 and two hours of hydrolysis time resulted in the production of NCC with 30% yield and with particle size ranging between 200 nm and 400 nm.

In recent years, NCC has been investigated as a filler or reinforcement material in polymer matrices, including polyvinyl alcohol (PVA), polylactic acid (PLA), polyvinyl chloride (PVC) and natural rubber foam.[13-17] However, no previous work has been reported on the

application of NCC as a reinforcement in nitrile butadiene rubber (NBR). To date, various rubbers have been used to produce rubber gloves, for example, natural rubber and synthetic rubber, such as NBR.[13] However, these materials, especially nitrile rubber, come with several drawbacks, including poor mechanical properties, conducing to susceptibility to being torn off, poor tensile properties, low robustness and non-degradability. To improve the mechanical properties of the rubber, the incorporation of fillers or reinforcement agents, including carbon black, silica, clay, rice bran carbon, nano-Fe_3O_4, zinc dimethacrylate, and other materials, has been investigated and it was demonstrated to enhance the rubber performance in terms of tear and tensile strength, hardness and degradability.[18-22] However, the reinforcement with such fillers still presents some disadvantages, as the fillers used are not environmentally friendly. Also, the addition of nano-Fe_3O_4 leads to a decline in the modulus of elongation and tensile strength of the material.[22] Notably, NCC is a promising reinforcement agent due to its biological origin, its low density and non-toxicity.

In this study, NCC was produced by the acid hydrolysis method, and was then used as reinforcement of a NBR matrix. This study investigated the effect of different concentrations of HCl on the yield, morphology, crystallinity, thermal properties and active surface area of NCC. Furthermore, the NBR composites were evaluated in terms of mechanical properties and morphology. This study aims to gain knowledge regarding the effect of different concentrations of HCl on the properties of NCC, and the influence of thus-produced NCC used reinforcement of NBR on the mechanical properties of the prepared composites.

EXPERIMENTAL

Materials

Commercially available cotton linter microcrystalline cellulose (MCC), with a diameter of 20 µm and length of several micrometers, extracted from tunicin, HCl (37 wt%), NBR latex (density 1.3 g/cm^3, solid content 43%) and other chemicals were purchased from Friendemann Schmidt and local suppliers.

Synthesis of NCC

MCC (5 g) was manually added to different concentrations of HCl acid (1M, 2M, 3M, 4M, 5M and 6M). The MCC solution was then hydrolyzed at 100 °C for 60 min, with continuous stirring (500 rpm) in a conical flask. Then, the mixture was quenched in an ice tube to stop the reaction. The reaction mixture was rinsed with distilled water and centrifuged for 30 min at 3000 rpm. The supernatant was replaced by new distilled water and centrifuged again for five times. The product was then dialysed using a dialysis tube and immersed in distilled water (for ion exchange) until the pH of the water reached equilibrium at pH 7. The resulting suspension was then freeze-dried and kept at room temperature until preparing the NBR matrix composites.

Preparation of NBR/NCC composites

SDBS (12.9 phr), ZDBC (2.58 phr), sulphur (5.02 phr), ZnO (4.66 phr) and TiO_2 (6.45 phr) were mixed with 500 mL of NBR latex at room temperature. The mixture was left overnight under stirring. The total solid content was calculated and confirmed within 23% of the TSC target (distilled water was added in order to dilute the mixture solution until the TSC target was met). The pH was adjusted using an ammonia solution to achieve pH 9.0 for preventing the latex from coagulating.

The NCC produced with 5M of HCl was chosen as the most suitable for preparing NBR/NCC composites. The desired content of dried NCC (from 1 phr to 5 phr) was mixed with NBR latex and stirred vigorously (250 rpm) at room temperature for 30 min. The existing ammonia solution in the NBR prevented the latex from coagulating even though the latex was vigorously stirred. After that, the compounding of NBR/NCC with other ingredients was carried out in a beaker using a magnetic stirrer. The composite was prepared from the mixture of NBR and NCC using the dipping tank method. The NBR/NCC composite was cured in an oven at 125 °C for 20 min. By modifying the contents of NCC over the range of 0-5 phr, a series of NBR composites with a thickness around 8 mm were prepared and denoted as NBR control, NBR/NCC 1 phr, NBR/NCC 2 phr, NBR/NCC 3 phr, NBR/NCC 4 phr, and NBR/NCC 5 phr, respectively.

Characterization

Yield percentage

The yield of NCC was estimated as the weight of the oven dried NCC divided by the original weight of MCC before hydrolysis was conducted. The yield percentage of NCC was calculated by using Equation 1:

$$Y = \frac{Wn}{Wp} x100\% \quad (1)$$

where Y is the NCC yield, Wn is the weight of NCC, and Wp is the weight of the MCC prior to hydrolysis.

Particle size analysis

Particle size analysis was conducted by dynamic light scattering (DLS) using a Zetasizer NanoZS Instrument (Malvern, UK) under the following conditions: dispersant water, material refractive index

1.47, dispersion refractive index 1.33, viscosity 0.8872 cP and temperature 25 °C. The general calculation model was used for irregular particles. Three measurements of 12 s each were carried out to calculate an average of the particle size and surface area.

Fourier transform infrared (FTIR) spectroscopy

FTIR spectra were recorded on a Thermo Nicolet FTIR spectrometer (Nicolet 6700, USA) within the range of 400-4000 cm^{-1}, at a spectral resolution of 4 cm^{-1}; 32 scans of each sample were recorded. Each sample was palletized with KBr powder.

X-ray diffraction (XRD) analysis

X-ray diffraction (XRD) data were collected by an X-ray diffractometer that was equipped with Cu Kα radiation (λ = 0.1541 nm) at the operating voltage and current of 45 kV and 100 MA, respectively. Diffractograms were collected in the 2θ range of 5~40 at the rate of 1 °/min with a resolving power of 0.05°.

The crystallinity index was calculated according to Equation 2:

$$\mathbf{CrI} = \frac{I_{002} - I_{am}}{I_{002}} \; X \; 100 \qquad (2)$$

where I_{002} is the overall intensity of the peak at 2θ of about 22° and I_{am} is the intensity of the baseline at 2θ of about 18°.

The crystallite size (L) of NCC was calculated, by using Scherrer's equation, as shown in Equation 3:

$$\mathbf{L} = \frac{K\lambda}{\beta cos\theta} \qquad (3)$$

where K is a constant of value 0.94; λ is the X-ray wavelength (0.1542 nm); β is the half height weight of the diffraction band (FWHM is full width at half maximum); and θ is the Bragg angle corresponding to the (200) plane.

Transmission electron microscopy (TEM) analysis

Drops of 0.001% of NCC suspensions were deposited on glow-discharged carbon-coated TEM grids. The specimen was negatively stained with 2% uranyl acetate, prior to complete drying and observed using a Philips CM200 electron microscope, operating at 200 kV. Images were recorded on Kodak SO163 film.

Thermogravimetry analysis (TGA)

The thermogravimetric analysis (TGA) was conducted using a GA Q500 (TA instruments, USA). Approximately 5 mg of sample was heated from 30 °C to 600 °C at a heating rate of 10 °C/min under nitrogen atmosphere.

Differential scanning calorimetry (DSC) analysis

DSC analysis was performed on a DSC-Q200 instrument under nitrogen atmosphere at a heating rate of 10 °C min^{-1} and flow rate of 50 mL/min. About 2 mg of each sample was placed in hermetically sealed DSC crimp pans, which were tested over the temperature range from 25 to 450 °C.

Mechanical tests

The tensile test was carried out by using a Universal Testing Machine. The samples were cut to dog bone shapes. All the experiments were carried out at room temperature with a crosshead speed of 500 mm/min according to ASTM D412. The tear test was performed according to ASTM D624.

Field emission scanning electron microscopy (FESEM) analysis

The surfaces of the NBR/NCC composites were analyzed by a field emission scanning electron microscope (FESEM), at voltage acceleration of 5 kV and low vacuum. Magnification of 10000x was used.

RESULTS AND DISCUSSION

Percentage yield, particle size distribution and zeta potential of NCC

As the concentration of HCl was increased from 1M to 6M, the total yield of NCC was significantly reduced from 93.94% to 73.24%. Higher yield could be seen at a low acid concentration, while the diameter and length of NCC were higher and more diverse. Thus, the average yield of NCC was reduced with the increase in the acid concentrations from 1M of HCl (93.94%), to 2M (92.81%), 3M (88.34%), 4M (87.32%), 5M (82.50%) and 6M (73.24%), as shown in Figure 1. Due to the high acid concentration, the cellulose is fully depolymerized and converted into amorphous nanoparticles in water.[23] At high acid concentration and temperature, the crystalline structure of NCC collapses and is reduced to sugars or further decomposition occurs into acid hydrolysis by-products.[24]

The particle size distribution and zeta potential results are also presented in Figure 1. The NCC synthesized using 1M HCl, produced with an average yield of 32.1%, had a particle size around 141.8 nm. No significant size reduction was recorded as the acid concentration was increased to 2M. The particle size was reduced to 122.4 nm as the acid concentration was increased to 3M. An approximately 43.5% yield of NCC was recorded at the acid concentration of 4M, with a particle zise of 105.7 nm. As the acid concentration was further increased to 5M, it led to a yield of 32.4% and a particle size of 91.28 nm, followed by a yield of 20.7% and a particle size of 164.2 nm at an acid concentration of 6M. This is explained by the conversion of most of the cellulose particles to

glucose (simple monomer units of cellulose), thus yielding NCC with a large diameter. Overall, these findings were in agreement with the results of FTIR and XRD analyses.

The surface charge of NCC decreased from -0.697 mV to -17.4 mV with the increasing concentration of the acid, followed by a slight increase to -14.8 mV at 6M concentration of HCl. It was also found that the suspension of NCC was considered unstable, with an absolute value lower than -25 mV. At 5M concentration of HCl, the surface charge was observed to drastically change from -0.938 mV to -17.4 mV. The zero value of surface charge resulted in a higher tendency to form agglomerates between the NCC particles. Under normal conditions, a value lower than -15 mV indicates the onset of agglomeration, while a value higher than -30 mV indicates that sufficient mutual repulsion among particles, which results in colloidal stability.[16] The HCl treated NCC crystals formed loose aggregates in water medium due to van der Waals forces and lack of surface charge of NCC. The interaction taking place among the colloidal particles in suspensions played an important role in determining the properties of NCC. These interactions involved intra/inter hydrogen bonding and van der Waals forces present among the polymeric chains. However, as the van der Waals interactions were weaker than the interactions between the hydrogen bonds, fluctuations in the distribution of the surface charge of NCC occurred.[25,26] Intensive interaction among the particles of NCC led to the formation of loose and bulky aggregates in the molecular structure. Higher agglomeration was due to the surface charge, as shown in Figure 1. Thus, the 1M sample with -0.697 mV surface charge was larger compared to the 5M sample. Nevertheless, no significant changes were observed in samples 1M and 2M in terms of surface charge, which contributed to insignificant changes in size distribution. Most of the reductions in surface charge led to notable changes in samples 3M to 5M. Figure 2 illustrates the hydrogen bonding in NCC during the hydrolysis.

Fourier transform infrared (FTIR) spectroscopy analysis

Figure 3 (a) and Table 1 present the FTIR spectra of NCCs synthesized with different concentrations of HCl catalyst. A strong, broad peak is observed in the 3500 cm^{-1} region due to the O-H bond stretching vibration.[27] It is explained by the intra- and inter-hydrogen bonding of NCCs.[28] A significant increase in the peak intensity is noted with increasing HCl concentration from 1M to 5M. This peak was then reduced at 6M concentration of HCl because of less surface activity. Excessive hydrolysis at a high concentration of acid led to the decomposition of NCC into glucose monomer units. The hydrolysis of MCC with 6M of HCl would lead to a small quantity of NCC produced, while the remaining HCl would be present in the glucose monomer. The active surface of NCC would be reduced, leading to the development of less active hydrogen bonds. The C-H vibration is noted at 2900 cm^{-1}, and is due to the presence of $–CH_2$ moieties in the NCC samples. The peak at 1644 cm^{-1} is associated with the O-H bonding due to the moisture content of the sample.

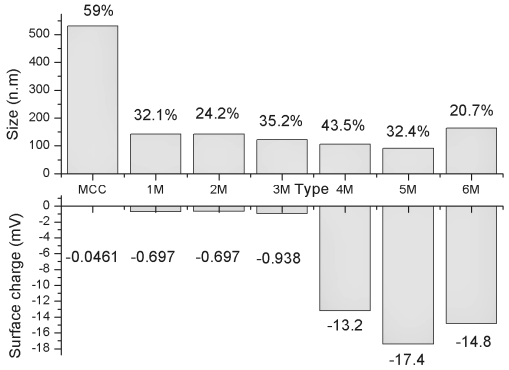

Figure 1: Percentage yield, particle size (above) and surface charge (below) of NCC at different concentrations of HCl (1M to 6M)

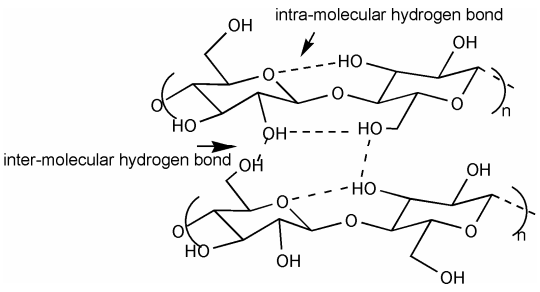

Figure 2: Hydrogen bonding between NCCs

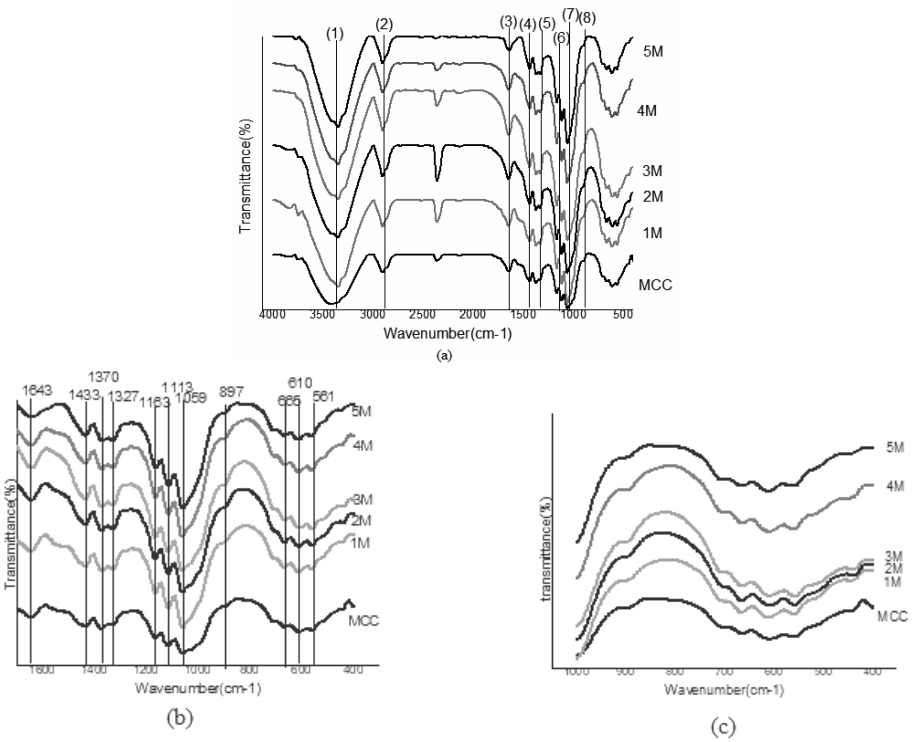

Figure 3: FTIR spectra of MCC and NCCs in different wavelength ranges, (a) 4000-400 cm^{-1}; (b) 1700-400 cm^{-1}; (c) 900-400 cm^{-1}

Table 1
Infrared spectra with assignments of different peaks

No	Peak position, cm^{-1}	Peak assignments
1	3416-3346	O-H stretching, vibration (hydrogen bonded)
2	2901-2904	C-H stretching vibration
3	1642-1644	Adsorbed water or moisture
4	1370	C-H bending or assymetric C-H deformation
5	1327-1332	C-H deformation and C-OH deformation
6	1164	C-O-C asymmetric valence vibration
7	1058-1059	C-O ether vibrations, methoxyl and β-O-4
8	897	C-H out of plane in position ring stretching in cellulose due to β-linkage

Although the NCC samples were thoroughly dried using the freeze-drying method, the elimination of all moisture was a challenging process. Moreover, the presence of the peak at 1433 cm^{-1}, which was due to CH_2 bending motion in cellulose, suggested the intermolecular hydrogen attraction of the C6 group.

The peak at 1372 cm^{-1} for MCC then shifted to 1370 cm^{-1} after acid hydrolysis due to C-H bending or asymmetric C-H deformation of polysaccharides, while the peak at 1332 cm^{-1} for MCC shifted to 1329 cm^{-1} (1M), 1328 cm^{-1} (2M), 1328 cm^{-1} (3M), 1327 cm^{-1} (4M), and 1327 cm^{-1} (5 M). As a result of CH_2 wagging, this peak shifted to a higher wavelength for sample 6M (1335 cm^{-1}), leading to the decomposition of NCCs into a simple glucose monomer. Then, the peak at 1164 cm^{-1} indicates C-O antisymmetric stretching, while that at 1115 cm^{-1}, which is due to C-O and C-C stretching, shifted to a lower wavelength (1113 cm^{-1}) after hydrolysis. A sharp peak is observed from 1053 cm^{-1} (MCC) to 1058 cm^{-1} (6M) is due to the C-O-C pyranose ring stretching vibration. An increase in this band would be associated with an increase in the cellulose content, indicating lower cellulose content in the sample 6M. Also, all the samples showed the peak at 897 cm^{-1} associated with β-

glycosidic linkages consisting of C_1-H and O-H bending typical of the cellulose structure. In the case of the region around 900 cm^{-1} (Fig. 3 (c)), changes are noted as a function of the concentration of the acid from 1M to 6M HCl. This peak became sharper and narrower with the increase in the molar concentration of the acid, because of the reduction in the glycosidic linkage, as MCC was broken down to glucose units.

X-ray diffraction (XRD) analysis

The main peaks of all the samples were observed at 14.7, 16.6, 22.8, and 34.1º (Fig. 4) due to the diffraction planes of (101), (10$\bar{1}$), (200) and (400), respectively.[29] This pattern is similar to that of native cellulose or cellulose I.[30] Two distinct crystalline structures are formed in cellulose I, namely cellulose Iα (triclinic) and cellulose Iβ (monoclinic). The amount of the crystalline structure depends on the source of cellulose, while cellulose Iβ is usually dominant in plants. The peaks at (101) and (10$\bar{1}$) are more pronounced when the crystalline content is high, suggesting that acid hydrolysis using HCl had a limited effect on the polymorphism of cellulose I for the produced NCC samples.

Generally, the NCC produced by acid hydrolysis can have lower crystallinity. Furthermore, a high concentration of the acid would result in faster hydrolysis of NCC and thus a harsher one. The reduction in the diffraction intensities of the amorphous region is attributed to the less structured and bulky region of NCC polymeric chains. Moreover, the capacity of NCC to hold water depends on its crystallinity as the volume of bound water decreases with the increase in the degree of crystallinity within the NCC molecules.[31,32] As seen in Figure 4, the X-ray diffraction patterns reflect a decrease in the crystalline domains of the NCC as a function of acid concentration. This is proven by the significant decrease in the intensity of the diffraction peaks at 22.8º for all the NCC samples. Based on the crystallinity index (CrI) of NCC shown in Table 2, the crystallinity of NCC was reduced with the increase in acid concentration from 1M to 6M HCl.

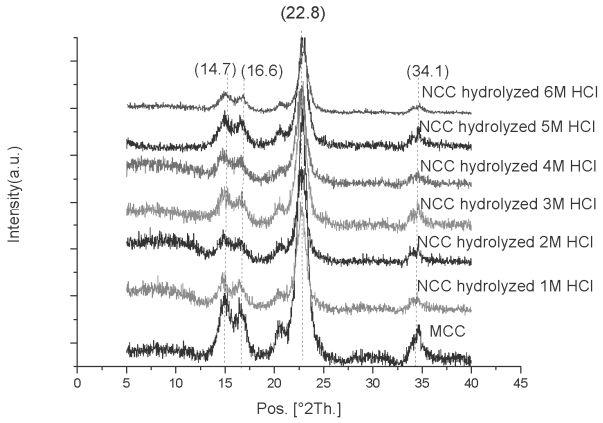

Figure 4: XRD patterns of MCC and NCCs (hydrolysed with 1M to 6M HCl)

Table 2
Bragg angle, FWHM, crystalline size and crystallinity index of NCCs prepared with different acid concentration

Type of sample	Bragg angle (degree)/d-spacing (Å)	FWHM (degree)	Crystallinity index	Crystallite size (nm)
MCC	3.864	0.984	69.49	8.2
NCC hydrolyzed with 1M HCl	3.878	0.984	73.89	8.2
NCC hydrolyzed with 2M HCl	3.888	0.984	71.40	8.2
NCC hydrolyzed with 3M HCl	3.880	0.984	72.15	8.2
NCC hydrolyzed with 4M HCl	3.883	0.984	71.03	8.2
NCC hydrolyzed with 5M HCl	3.896	1.181	70.50	6.9
NCC hydrolyzed with 6M HCl	3.901	1.808	64.78	4.5

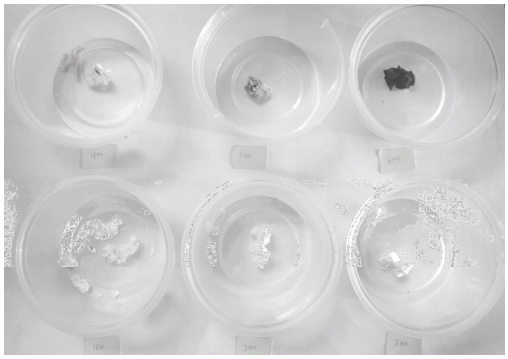

Figure 5: Color changes of NCCs after treatment with different acid concentrations from 1M to 6M HCl

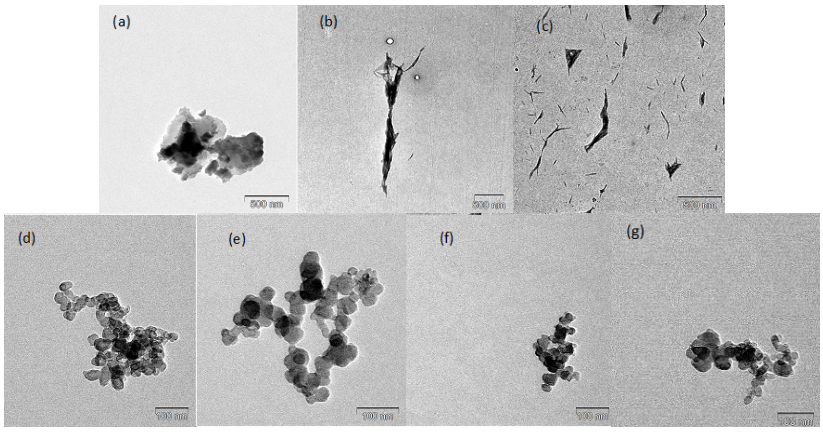

Figure 6: TEM images of (a) MCC (500 nm), (b) 1M (500 nm), (c) 2M (500 nm), (d) 3M (100 nm), (e) 4M (100 nm), (f) 5M (100 nm), (g) 6M (100 nm)

Figure 5 illustrates the changes in color from that of MCC to those of NCC treated with different contrations of HCl. Specifically, the darker color indicates the burning of NCC and its concersion into simple glucose units. This supports the choice of the acid concentration of 5M HCl as an optimized condition for the production of NCC. The successive removal of the amorphous region was observed during this reaction. At high temperature, the reaction occurred in the amorphous region at a higher rate, cleaving the β-1,4-glycosidic linkages by maintaining unaltered the crystallite segments.[33,34] The amorphous part was preferentially cleaved, while the crystalline regions were resistant to acid attack and mostly remained intact during hydrolysis.

However, the increase in acid concentration from 2M to 5M led to a slight decrease of the crystallinity index because of partial destruction of the crystalline structure and production of more disordered regions in nanocellulose. Further decrease in crystallinity was observed at 5M and 6M HCl concentrations, which was proportional to the decrease in the crystal size. At 6M HCl, the crystallinity index and crystallite size were reduced to 64.78 and 4.5 nm, respectively, because of extensive degradation of NCC caused by the high concentration of HCl, while most NCCs were converted into glucose. This finding is in agreement with those reported in a previous study by Li *et al*.[35]

Transmission electron microscopy (TEM) analysis

Transmission electron micrographs of MCC and NCCs synthesized with different concentration levels of HCl are presented in Figure 6. As may be noted in Figure 6a, the MCC has large dimensions and particles are contoured from dark color to white. Specifically, the dark color indicates a thicker structure, compared to the white one, due to agglomeration of MCC. Meanwhile, based on Figure 6b and Figure 6c,

which present needle-like and narrow shapes, it can be concluded that the treatment with 1M and 2M HCl would hydrolyze MCC into NCC, with a variety of sizes and shapes. The treatment with 3M HCl (Fig. 6d) modified the NCCs produced to smaller particulate sizes, with no significant variation. The difference in the NCC shapes is observed when comparing the NCCs produced with 1M to 6M acid catalyst concentration.

Further observation was conducted on the platelet-like particles of the NCC, those achieved at higher concentration levels of the acid (Figs. 6 (d-g)). After hydrolysis, the NCC was found to aggregate due to the hydrogen bond interactions *via* the surface hydroxyl groups. Moreover, the effect of the interfacial interaction and bonding could be amplified in the NCC particles with a larger specific surface area. The specific surface area increases with a rising aspect ratio or reduced diameter of NCC. The NCC that has a larger surface to volume ratio is more suitable for application in reinforcing composites as it can provide more contact surface and improved surface reactivity towards the polymer matrix, effectively preventing polymer chains mobility.[36] Due to increased interfacial interaction, improved properties of composites, with the use of low filler conten, could be predicted. However, due to the highly hydrophilic nature of cellulose, NCC particles with high surface area might attract surrounding nano-sized particles, forming agglomerates.[11] When aggregation occurs, re-dispersing the NCC would be a challenging process, thus such particles would not be suitable for reinforcement purposes, without any modification treatment or functionalization.

Thermogravimetry analysis (TGA)

Figure 7 and Figure 8 illustrate the TG and DTG thermograms of MCC and NCCs produced with various HCl concentration levels. The degradation patterns were quite similar for all the samples. As shown in Figure 7a, the first weight loss occurred at a temperature <100 °C. All the samples, from MCC to NCCs, demonstrated a small weight loss in this region due to the evaporation of absorbed water (Fig. 7b). As may be noted, as an effect of excessive hydrolysis, the NCC produced with 6M HCL was mostly converted into glucose monomer and had high amorphous content; therefore, it had a higher tendency to absorb moisture and thus presented higher weight loss. This finding was in agreement with the report of Mariano *et al*.[37]

The region ranging from 100 °C to 200 °C demonstrated constant weight for the different types of NCCs. The degradation onset temperature was recorded at 322 °C for MCC, it slightly increased to 327 °C for 1M HCl hydrolyzed NCC, then decreased to 324 °C, and remained constant for the NCCs obtained with 2 M, 3 M, 4 M and 5M HCl. Subsequently, the onset temperature dropped to 320 °C for the NCC treated with 6M HCl. For all the samples, from MCC and the whole range of NCCs, the dominant peak was recorded between 300 °C and 350 °C, a temperature range where degradation processes, such as depolymerization, dehydration and decomposition of glycosidic linkage and rings, take place. The decomposition that occurred beyond 350 °C consisted in the oxidation and breakdown of the charred residue into gaseous products with low molecular weight.

It was reported by Zhou *et al*.[38] that the decomposition temperature of cellulose ranges from 315 °C to 400 °C, which is in line with the findings of this study. Lower onset was reported by Flauzino *et al*.,[39] who performed the conversion of MCC to nanocrystals with sulfuric acid. They explained the lower onset as being caused by the presence of sulfate groups on the cellulose surface, which had a catalytic effect on the thermal degradation of cellulose. Moreover, the decomposition at a lower temperature would also result in a faster transfer of heat in the samples. Subsequently, a difference in the amount of weight loss occurred, indicating the degradation of the samples started within the heating region. As seen in the final degradation stage at 400 °C, the MCC weight loss only remained at 17.08%, compared to the other samples. Specifically, the NCCs synthesised with 1M, 2M, 3M, 4M, 5M and 6M acid recorded 15.32%, 14.80%, 14.26%, 14.25%, 12.26% and 14.97% respectively. The highly crystalline structure of NCCs was a key factor in the thermal stability of the samples, as the cellulose chains remained in a highly ordered formation through strongly stabilized hydrogen bonding.[3] The formation of highly ordered three-dimensional crystal structures is considered to lead to high thermal stability, as the interchain hydrogen bonds in the crystalline regions are not easily dissociated by high temperature, preventing the cellulose from degradation.[40]

The DTG thermograms in Figure 8 (a, b) illustrate that the maximum peaks exhibited by MCC reached 348 °C, while those of NCC

reached 352 °C (1M HCl), 349 °C (2M HCl), 348 °C (3M HCl), 349 °C (4M HCl), 348 °C (5M HCl) and 345 °C (6M HCl). The highest thermal stability was exhibited by the NCC hydrolyzed with 1M HCl, as shown by its highest temperature peak.

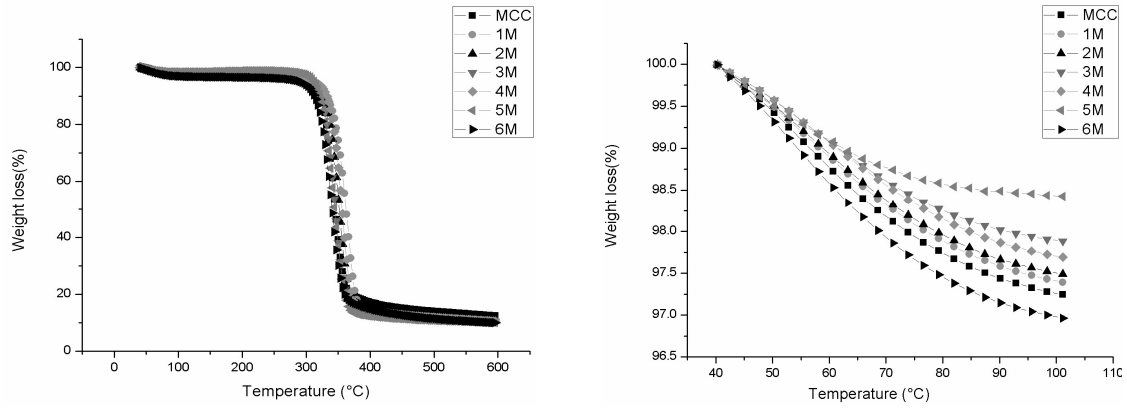

a) b)

Figure 7: TG curves for NCC samples (30-600 °C) (a) and their magnification in the region 0-100 °C (b)

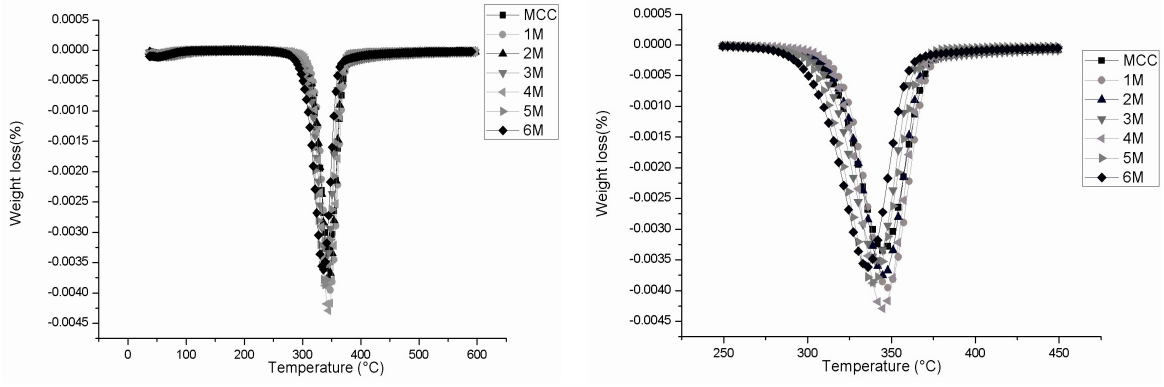

a) b)

Figure 8: DTG curves for NCC samples (30-600 °C) (a) and their magnification in the region 250-410 °C (b)

Table 3
Thermal degradation parameters of different NCC samples

Sample type	Onset temperature (°C)	Weight loss (%)	T_{max} (°C)	Char yield (%)
MCC	322	96.50	348	12.47
NCC hydrolyzed with 1M HCl	327	96.50	352	11.43
NCC hydrolyzed with 2M HCl	324	96.79	349	11.22
NCC hydrolyzed with 3M HCl	324	98.04	348	10.42
NCC hydrolyzed with 4M HCl	324	97.01	349	10.40
NCC hydrolyzed with 5M HCl	324	98.01	348	10.06
NCC hydrolyzed with 6M HCl	320	97.52	345	10.01

Note: T_{max}: degradation temperature from DTG curve, and char at 600 °C

The amount of char residue was reduced with the increase in molar concentration of the acid used during the hydrolysis process. As shown in Table 3, the amount of char for MCC was 12.47%, and it decreased to 11.43% for 1M, 11.22% for 2M, 10.42% for 3M, 10.4% for 4M, 10.06% for 5M and 10.01% for 6M HCl. Insignificant differences in the amount of char residue are noted among the samples treated with 3M and 4M HCl.

The reduction in the char residue, with an increased molar concentration of HCl, for the NCC samples, can be explained by increased hydrogen bonding, which was broken down through acid hydrolysis. The split in hydrogen bonding would contribute to the formation of larger surface area, which could easily be degraded by the thermal reaction.[41] In another study, by Meyabadi *et al*.,[10] it was reported that the amount of charred residue was higher in samples with higher crystallinity. The increase in the concentration of HCl would provide more H^+, which would strengthen the catalytic reaction of the glycosidic bonds between the nanocrystalline cellulose chains. This mechanism of hydrogen bond splitting is illustrated in Figure 9.

Differential scanning calorimetry (DSC) analysis

Figure 10 illustrates the DSC of MCC and NCCs hydrolyzed different concentrations of HCl. The DSC patterns appear to be similar for all the samples. The first endotherm took place in the temperature range from 33 °C to 118 °C for MCC, from 31 °C to 113 °C (1M), from 32 °C to 116 °C (2M), from 34 °C to 116 °C (3M), from 34 °C to 114 °C (4M), from 34 °C to 109 °C (5M), and from 41 °C to 116 °C (6M) for the NCCs obtained with different concentrations of HCl. The endotherm in this range was the result of water evaporation or degradation of low molecular weight and amorphous components.[42] The rearrangement of molecular chains of the amorphous component would increase the endotherms transition.[43] Meanwhile, the second endotherm transition occurred in the temperature range from 312 °C to 362 °C for MCC, and from 333 °C to 369 °C (1M), from 320 °C to 355 °C (2M), from 314 °C to 351 °C (3M), from 309 °C to 353 °C (4M), from 310 °C to 351 °C (5M), and from 299 °C to 317 °C (6M) for the NCCs hydrolyzed with different concentrations of HCl. This endotherm transition could be attributed to the decomposition of the crystalline part of NCC. In the case of the NCC, this region corresponded to the melting temperature where the separation of glycosidic bonds and the depolymerization of cellulose chains occur.[43] A sharp endothermic peak in this region is assigned to the fusion of the crystalline parts, the peak of MCC reaching 322 °C, while those of the NCCs – 355 °C (1M), 339 °C (2M), 333 °C (3M), 334 °C (4M), 331 °C (5M), and 327 °C (6M HCl). The decrease in the peak temperature in this region could be explained by the increase in the amorphous content and the reduction in the cellulose crystallite size.[42]

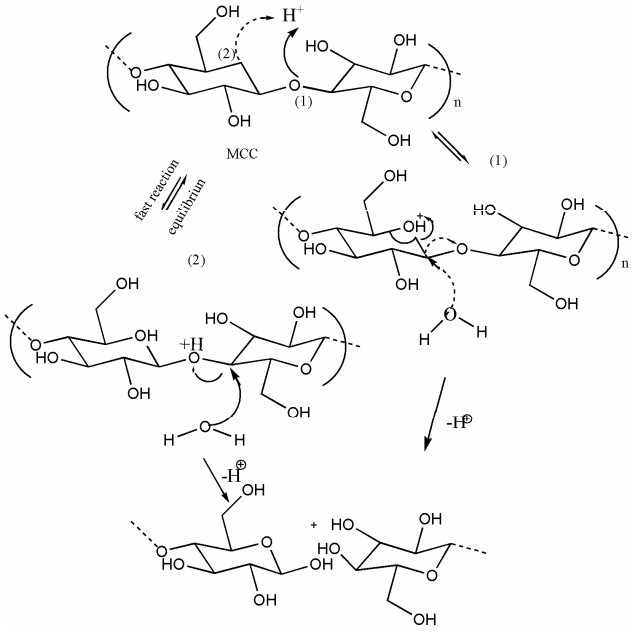

Figure 9: Acid hydrolysis mechanism[11]

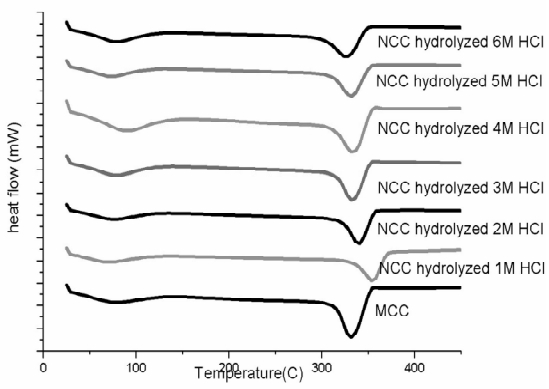

Figure 10: DSC curves of MCC and NCCs

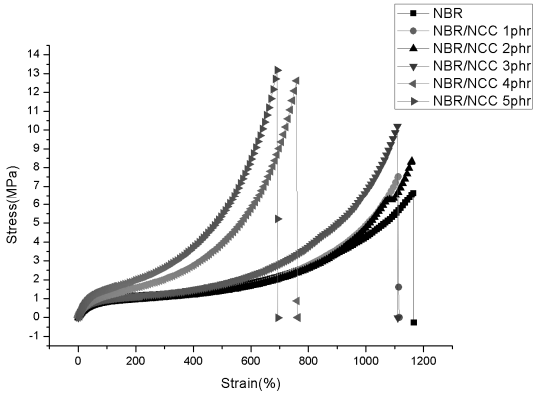

Figure 11: Stress-strain curves of NBR and NBR/NCC composites

Table 4
Mechanical properties of NCC reinforced NBR composites

NCCs content (phr)	Tensile strength (MPa)	Modulus at 100% strain (MPa)	Modulus at 300% strain (MPa)	Modulus at 500% strain (MPa)	Elongation at break (%)	Tear strength (kN/m)
0	8.264(1.07)	1.057 (0.18)	1.346(0.28)	1.680(0.48)	3.457(0.65)	15.008 (1.85)
1	8.780(0.78)	0.871 (0.08)	1.213(0.09)	1.646(0.12)	2.937(0.32)	14.714 (1.23)
2	7.259(1.46)	0.840 (0.03)	1.106(0.04)	1.402(0.06)	2.807(0.14)	14.808 (1.61)
3	9.105(2.15)	0.983 (0.06)	1.272(0.09)	1.674(0.11)	3.315(0.23)	14.020 (0.78)
4	13.608(1.65)	1.173 (0.04)	1.909(0.07)	3.392(0.14)	3.504(0.13)	13.106 (0.74)
5	16.588(3.06)	1.597 (0.11)	2.753(0.22)	5.408(0.42)	4.539(0.34)	15.458 (1.21)

Note: Standard deviations are shown in brackets

Mechanical properties

The stress-strain curves of the NBR/NCC composites are illustrated in Figure 11, while the mechanical performance of the composites is demonstrated in Table 4. Notably, the stress-strain curves shown in Figure 11 are similar to the pattern observed by Kumagai *et al*.[44] The increase in stress was due to the strain-induced crystallization at a higher strain level in the composite. Further improvement could be seen from the tensile strength result with the addition of 1 phr to 5 phr NCC to the NBR composites.

Compared to the control NBR, a slight decrease in the composite containing 2 phr NCC was due to the incompatibility or agglomeration of NCC in the NBR matrix, although this decrease was not significant. Moreover, the tensile strength for the 4 phr and 5 phr composite samples was more significant, compared to the tensile strength of the NBR control sample. Although the mean of the 5 phr sample was the highest, there was no substantial difference between the mean of the 5 phr and that of the 4 phr samples.

When comparing the tensile strength of the NBR/NCC composites designed in this study for manufacturing rubber gloves with that of commercial gloves made from the fully synthetic NBR, the minimum tensile strength for the commercial product is 22 MPa, which is higher than the tensile strength the composites in our study. Also, Chen *et al*.[13] reported on foamed nitrile rubber reinforced with cellulose nanocrystals, suggesting that the 15 phr cellulose nanocrystals was the optimum value to fill in nitrile foam rubber to achieve a tensile strength of 6.54 MPa. As foamed rubber consists of a high quantity of voids, it was suggested that better mechanical properties of foamed rubbers could be achieved through smaller foam size. It was also proposed by Chen *et al*.[13] and Cao *et al*.[45] that low loadings of the NCC filler in the matrix could improve the mechanical properties of rubber composites.

The effects of filler loading on the modulus at 100% elongation (M100) are illustrated in Table 4. It may be noted that M100 increased with rising NCC content from 1 phr to 5 phr. The increase in M100 for the 1 phr to 5 phr samples was due to the improvement in the cross-linking of the NBR matrix with NCC. The incorporation of NCCs into the NBR matrix increased the stiffness of the material and thus the tensile modulus. Notably,

better dispersion could enhance the interfacial adhesion between the NCCs and the NBR matrix. Based on the morphological study, it was suggested that the NCC developed interfacial bonding with the NBR matrix. However, compared to the neat NBR (control), no significant increment in the modulus at 300% and 500% strain was noted in the samples containing 1 phr to 3 phr NCC. Meanwhile, the value of the modulus at 300% and 500% strain for commercial gloves amounts to 0.8 MPa and 1.5 MPa, respectively, and thus, compared to them, the NBR/NCC composites in this study reached higher values for both moduli, and for both the increment was proportional with the addition of NCC to NBR. The incorporation of 1 phr to 3 phr NCC led to minor effects on the cross-linking with the NBR network, therefore, no improvement was achieved. However, a significant increment is noted upon NCC addition of 4 phr and 5 phr, due to the strong network interaction developed between the rubber and the filler. The tensile strength and modulus of elasticity were higher than those of NBR upon the addition of 4 phr and more filler. As the elastic modulus represents the ability of materials to resist deformation, the increase in the elastic modulus of the composites indicated stronger resistance to deformation.[46]

Table 4 illustrates the elongation at break for NBR and NBR composites at different filler loadings. Based on the results in Table 4, it could be seen that the 5 phr NCC loading led to the highest elongation at break, while the 2 phr one showed the lowest elongation at break. The addition of 5 phr filler could improve the elongation at break of NBR, due to improved cross-linking between NBR and NCC. No significant difference can be seen for the 1 phr to 4 phr loadings, when compared to NBR (control), as at these loadings the agglomeration of NCCs in the matrix occurred because of the strong hydrogen bonding between the NCCs. As a result, a brittle composite was formed, with low elongation at break. Overall, this finding is in agreement with Venugopal *et al*.,[47] who concluded that agglomeration at higher loadings impacted tensile strength and tear strength. The flexibility and elasticity of the rubber chains were restricted when the NCCs were incorporated into the NBR matrix, leading to a more rigid rubber matrix and to a reduction of the elongation at break. Nevertheless, the tear strength results in Table 4 were not significantly different with the increase in the NCC loading. Upon comparison with commercial gloves (54 kN/m), the results obtained indicate that the tear strength of NBR/NCC composites was lower than that of commercial gloves. The addition of NCC could not stop the propagation of cracks, initiated by the tearing force. The interaction mechanism of NCC and NBR is illustrated in Figure 12.

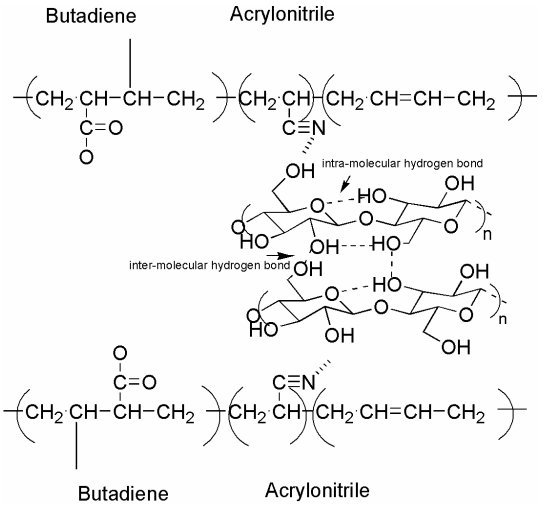

Figure 12: Interaction of NCC with NBR matrix

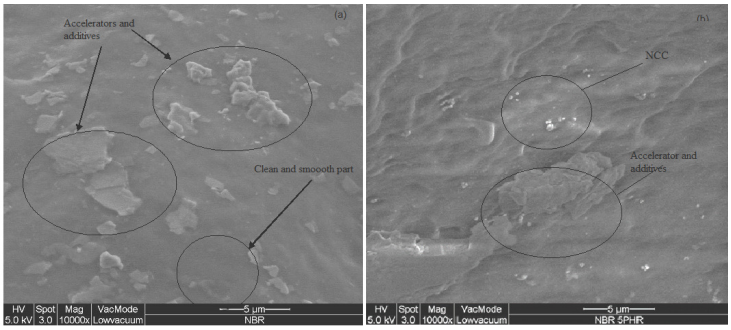

Figure 13: FESEM images of (a) NBR control and (b) NBR/NCC composites at 5 phr filler loading

Morphological study by Field Emission Scanning Electron Microscopy (FESEM) analysis

Figure 13 presents images of the surface of the neat NBR and the composite with 5 phr loading. In Figure 13 (a), the micrograph illustrates the surface of the neat NBR, indicating strong interfacial adhesion and effective wetting in the rubber blend. The unmodified NBR taken as a control sample presents a smooth surface, with some protruding elements, possibly originating from the accelerator and additives.

After NBR was reinforced with NCC, some NCC particles are observed represented by white dots. Increased NCC loading is conducive to the aggregation or agglomeration of NCC particles and leads to poor dispersion in the NBR matrix, which resulted in poor performance of the material. Also the hydrophilic/hydrophobic difference of NCC and NBR would result in incompatibility problems. Such incompatibility could affect the performance of NBR composites, when the NCC is incorporated at higher loading. Thus, uniform distribution of the filler within the matrix would create further crosslinking between the NCCs and the NBR, while, in contrast, the agglomeration of the filler and its poor distribution in the matrix could deteriorate the interfacial adhesion and bonding within the composites produced.

CONCLUSION

NCC was successfully extracted through the hydrolysis of commercial microcrystalline cellulose cotton linter. The effect of HCl concentration on the yield percentage, particle size, functional groups, crystallinity and thermal stability of NCC was studied. It was found that, although the yield percentage was reduced with increased concentration of the acid, it also impacted the size of the NCC produced. Moreover, the crystallinity of NCC exhibited reduction at higher HCl concentrations, because of the separation of the glycosidic linkage and the decrease in crystallite size. Consequently, the thermal stability of the NCC produced with higher concentration of HCl was lower. Considering all the parameters, it was considered that the optimum acid condition for hydrolysis was 5M HCl.

Based on the analysis of the composite materials prepared by incorporating NCCs with different loadings, it was found that the tensile strength exhibited a significant improvement in the materials containing up to 5 phr NCC loading. The tensile modulus at 100%, 300%, 500% strain, and the elongation at break improved with the incorporation of NCC as a filler. In conclusion, the reinforcement of NBR composites with NCC can improve the mechanical performance of the composites.

ACKNOWLEDGEMENTS: The authors would like to thank the University of Malaya for providing financial support of this project. This project was financially supported by Postgraduate Research Grant (PPP) (PG238-2015A: Effects on surface acetylated nanocrystalline cellulose (NCC) reinforced in nitrile butadiene rubber (NBR) composite) and SATU Research Grant 2019 (ST011:2019 Development of biodegradable and high strength composites).

REFERENCES

[1] S. Elazzouzi-Hafraoui, Y. Nishiyama, J.-L. Putaux, L. Heux, F. Dubreuil *et al*., *Biomacromolecules*, **9**, 57 (2007), https://doi.org/10.1021/bm700769p

[2] B. Peng, N. Dhar, H. Liu and K. Tam, *Can. J. Chem. Eng*., **89**, 1191 (2011), https://doi.org/abs/10.1002/cjce.20554

[3] S. Rebouillat and F. Pla, *J. Biomater. Nanobiotechnol.*, **4**, 165 (2013), https://doi.org/10.4236/jbnb.2013.42022
[4] K.-Y. Lee, Y. Aitomäki, L. A. Berglund, K. Oksman and A. Bismarck, *Compos. Sci. Technol.*, **105**, 15 (2014), https://doi.org/10.1016/j.compscitech.2014.08.032
[5] M. L. Yan, S. J. Li, M. X. Zhang, C. J. Li, F. Dong *et al.*, *Bioresources*, **8**, 6330 (2013), https://ncsu.edu/bioresources/BioRes_08/BioRes_08_4_6330_Yan_LZLDL_Charac_Acetylated_NCC_SingleStep_3771.pdf
[6] Y. J. Tang, S. J. Yang, N. Zhang and J. H. Zhang, *Cellulose*, **21**, 335 (2014), https://doi.org/10.1007/s10570-013-0158-2
[7] H. Sadeghifar, I. Filpponen, S. P. Clarke, D. F. Brougham and D. S. Argyropoulos, *J. Mater. Sci.*, **46**, 7344 (2011), https://doi.org/10.1007/s10853-011-5696-0
[8] H. Kargarzadeh, I. Ahmad, I. Abdullah, A. Dufresne, S. Zainudin *et al.*, *Cellulose*, **19**, 855 (2012), https://doi.org/10.1007%2Fs10570-012-9684-6
[9] L. H. Zaini, M. Jonoobi, P. M. Tahir and S. Karimi, *J. Biomater. Nanobiotechnol.*, **4**, 37 (2013), https://doi.org/10.4236/jbnb.2013.41006
[10] T. F. Meyabadi, F. Dadashian, G. M. M. Sadeghi and H. E. Z. Asl, *Powder Technol.*, **261**, 232 (2014), https://doi.org/10.1016/j.powtec.2014.04.039
[11] P. Lu and Y.-L. Hsieh, *Carbohyd. Polym.*, **82**, 329 (2010), https://doi.org/10.1016/j.carbpol.2010.04.073
[12] D. Bondeson, A. Mathew and K. Oksman, *Cellulose*, **13**, 171 (2006), https://doi.org/10.1007/s10570-006-9061-4
[13] Y. Chen, Y. Zhang, C. Xu and X. Cao, *Carbohyd. Polym.*, **130**, 149 (2015), https://doi.org/10.1016/j.carbpol.2015.05.017
[14] B. Schyrr, S. Pasche, G. Voirin, C. Weder, Y. C. Simon *et al.*, *ACS Appl. Mater. Interfaces*, **6**, 12674 (2014), https://doi.org/10.1021/am502670u
[15] S.-Y. Lee, D. J. Mohan, I.-A. Kang, G.-H. Doh, S. Lee *et al.*, *Fiber. Polym.*, **10**, 77 (2009), https://doi.org/10.1007/s12221-009-0077-x
[16] J. Trifol, D. Plackett, C. Sillard, O. Hassager, A. E. Daugaard *et al.*, *J. Appl. Polym. Sci.*, **133**, 43257 (2016), https://doi.org/10.1002/app.43257
[17] Y. Zhou, S. Fu, L. Zheng and H. Zhan, *Express Polym. Lett.*, **6**, 794 (2012), https://doi.org/10.3144/expresspolymlett.2012.85
[18] C. H. Xu, Y. K. Chen, Y. P. Wang and X. R. Zeng, *Polym. Compos.*, **32**, 2084 (2011), https://doi.org/10.1002/pc.21239
[19] A. Mostafa, A. Abouel-Kasem, M. R. Bayoumi and M. G. El-Sebaie, *Mater. Des.*, **30**, 2721 (2009), https://doi.org/10.1016/j.matdes.2008.09.045
[20] S. I. Volfson, N. A. Okhotina, A. I. Nigmatullina and O. A. Panfilova, *AIP Conf. Proc.*, **1599**, 418 (2014), https://doi.org/10.1063/1.4876867
[21] S. H. Xu, J. Gu, Y. F. Luo, D. M. Jia and L. Yan, *Polym. Compos.*, **36**, 861 (2015), https://doi.org/10.1002/pc.23005
[22] Q. L. Wang, F. Y. Yang, Q. Yang, J. H. Chen and H. Y. Guan, *Mater. Des.*, **31**, 1023 (2010), https://doi.org/10.1016/j.matdes.2009.07.038
[23] Y. F. Liu, H. S. Wang, G. Yu, Q. X. Yu, B. Li *et al.*, *Carbohyd. Polym.*, **110**, 415 (2014), https://doi.org/10.1016/j.carbpol.2014.04.040
[24] D. Qiang, M. Zhang, J. Li, H. Xiu and Q. Liu, *Cellulose*, **23**, 1199 (2016), https://doi.org/10.1007/s10570-016-0858-5
[25] C. Salas, T. Nypelo, C. Rodriguez-Abreu, C. Carrillo and O. J. Rojas, *Curr. Opin. Colloid Interface Sci.*, **19**, 383 (2014), https://doi.org/10.1016/j.cocis.2014.10.003
[26] S. M. Notley, B. Pettersson and L. Wagberg, *J. Am. Chem. Soc.*, **126**, 13930 (2004), https://doi.org/10.1021/ja045992d
[27] A. R. Nair, S. Sambhudevan and B. Shankar, *Cellulose Chem. Technol.*, **53**, 263 (2019), https://www.cellulosechemtechnol.ro/pdf/CCT3-4(2019)/p.263-270.pdf
[28] V. Hospodarova, E. Singovszka and N. Stevulova, *Am. J. Anal. Chem.*, **9**, 303 (2018), https://doi.org/10.4236/ajac.2018.96023
[29] P. Mansikkamäki, M. Lahtinen and K. Rissanen, *Carbohyd. Polym.*, **68**, 35 (2007), https://doi.org/10.1016/j.carbpol.2006.07.010
[30] S. Park, J. O. Baker, M. E. Himmel, P. A. Parilla and D. K. Johnson, *Biotechnol. Biofuels*, **3**, 10 (2010), https://doi.org/10.1186/1754-6834-3-10
[31] K. Nakamura, T. Hatakeyama and H. Hatakeyama, *Text. Res. J.*, **51**, 607 (1981), https://doi.org/10.1177/004051758105100909
[32] A. Espert, F. Vilaplana and S. Karlsson, *Compos. A-Appl. Sci. Manuf.*, **35**, 1267 (2004), https://doi.org/10.1016/j.compositesa.2004.04.004
[33] W. Chen, H. Yu, Y. Liu, P. Chen, M. Zhang *et al.*, *Carbohyd. Polym.*, **83**, 1804 (2011), https://doi.org/10.1016/j.carbpol.2010.10.040
[34] X. Y. Tan, S. B. Abd Hamid and C. W. Lai, *Biomass Bioenerg.*, **81**, 584 (2015), https://doi.org/10.1016/j.biombioe.2015.08.016
[35] J. Li, X. Zhang, M. Zhang, H. Xiu and H. He, *BioResources*, **9**, 1334 (2014), https://ncsu.edu/bioresources/
[36] M. Minelli, M. G. Baschetti, F. Doghieri, M. Ankerfors, T. Lindström *et al.*, *J. Membrane Sci.*, **358**, 67 (2010), https://doi.org/10.1016/j.memsci.2010.04.030
[37] M. Mariano, N. El Kissi and A. Dufresne, *Carbohyd. Polym.*, **137**, 174 (2016), https://doi.org/10.1016/j.carbpol.2015.10.027
[38] L. Zhou, H. He, C. Jiang, Li Ma and P. Yu, *Cellulose Chem. Technol.*, **51**, 109 (2017), http://www.cellulosechemtechnol.ro/pdf/CCT1-2(2017)/p.109-119.pdf

[39] W. P. Flauzino Neto, M. Mariano, I. Souza Vieira da Silva, H. Alves Silvério, J.-L. Putaux *et al*., *Carbohyd. Polym*., **153**, 143 (2016), https://doi.org/10.1016/j.carbpol.2016.07.073
[40] G. H. D. Tonoli, E. M. Teixeira, A. C. Corrêa, J. M. Marconcini, L. A. Caixeta *et al*., *Carbohyd. Polym*., **89**, 80 (2012), https://doi.org/10.1016/j.carbpol.2012.02.052
[41] Y. Tang, X. Shen, J. Zhang, D. Guo, F. Kong *et al*., *Carbohyd. Polym*., **125**, 360 (2015), https://doi.org/10.1016/j.carbpol.2015.02.063
[42] J. I. Morán, V. A. Alvarez, V. P. Cyras and A. Vázquez, *Cellulose*, **15**, 149 (2008), https://doi.org/10.1007/s10570-007-9145-9
[43] L. C. Yeng, M. U. Wahit and N. Othman, *J. Teknol*., **75**, 107 (2015), https://doi.org/10.11113/jt.v75.533843
[44] A. Kumagai, N. Tajima, S. Iwamoto, T. Morimoto, A. Nagatani *et al*., *Int. J. Biol. Macromol*., **121**, 989 (2019), https://doi.org/10.1016/j.ijbiomac.2018.10.090
[45] X. Cao, C. Xu, Y. Wang, Y. Liu, Y. Liu *et al*., *Polym. Test*., **32**, 819 (2013), https://doi.org/10.1016/j.polymertesting.2013.04.005
[46] X. Xiong, Y. Bao, H. Liu, Q. Zhu, R. Lu *et al*., *Mater. Chem. Phys*., **223**, 535 (2019), https://doi.org/10.1016/j.matchemphys.2018.11.041
[47] B. Venugopal and G. Joyalatha, *Mater. Today*: *Proc*., **5**, 16724 (2018), https://doi.org/10.1016/j.matpr.2018.06.036